encit 2020

ABCM Associação Brasileira de Engenharia e Ciências Mecânicas

18th Brazilian Congress of Thermal Sciences and Engineering
November 16-20, 2020 (Online)

ENC-2020-0361
NUMERICAL SIMULATION OF FLUIDIZED BEDS WITH BONDED PARTICLES

Nicolao Cerqueira Lima
nicolaol@hotmail.com
Fernando David Cúñez
fernandodcb@fem.unicamp.br
Erick Franklin
franklin@fem.unicamp.br
School of Mechanical Engineering, UNICAMP - University of Campinas, Rua Mendeleyev, 200, Campinas, SP, Brazil

Abstract. *This research proposes a numerical study of the fluidization of non-spherical particles in confined pipes. The fluidized bed system presented here consists of an ascending water flow in a 25.4 mm-ID pipe with 300 aluminum beads of 4.8 mm diameter combined in a triangle configuration, forming 100 bonded particles. Bonded atoms can assume different formations and geometries, and, therefore, can characterizes problems found in several branches of industry. The results obtained for a flow rate of 250 L/h showed the formation of plugs that quickly jam inside the pipe. We compared our results with the ones observed in ongoing experiments and both are in good agreement. Other experiments are still being carried out concurrently with the numerical simulations, and will be eventually used to validate our numerical model.*

Keywords: *computational fluid dynamics (CFD), discrete element method (DEM), fluidized bed, bond, narrow pipes*

1. INTRODUCTION

Fluidization of a bed of solid particles is mainly dictated by the gas/liquid flow conditions and by the physical properties of the particles and the fluid. The transition between a packed bed and a fluidized one takes place for certain critical values of the controlling parameters. In the case of solid-liquid fluidized beds (SLFB) consisting of spherical particles, when the fluid velocity is increased above that for minimum fluidization (U_{mf}), for example, the system enters a uniform and homogeneous regime, something well-known and understood (Didwania and Homsy, 1981; Nicolas *et al.*, 1996). However, those regimes are seldom observed in practice. Most of processes involving fluidized beds operate with fluid velocities well above that for minimum fluidization and, in those cases, the system becomes unstable, with transverse waves, bubbles, or elongated bubbles being observed (Guazzelli, 2004).

Understanding the hydrodynamics and particle displacement during the flow is crucial for the development, design and optimization of fluidization processes. However, the physics of these systems and the singular phenomena arising from them are complex and often difficult to be observed experimentally. Therefore, numerical simulations have become an important tool to investigate the dynamics of fluidized beds by analyzing individual particle trajectories or by quantifying flow parameters, such as the velocity field or contact forces (Esteghamatian *et al.*, 2017; Cúñez and Franklin, 2019b). Over the years, several approaches have been used to describe the fluid-solid interactions. But methods based on the combination of the Discrete Element Method (DEM) with Computational Fluid Dynamics (CFD), also known as CFD-DEM, are commonly adopted (Deen *et al.*, 2007). In this approach, the fluid is treated as a continuous medium, while the particle phase treated as a discrete medium, being tracked through the calculated flow field. In addition, most of the works simplify CFD-DEM models by considering spherical particles. However, most particles in industrial processes are actually non-spherical or consist of more than one solid species. Recently studies have shown that the geometry and properties of the particles can influence the bed porosity, induce particle agglomeration, and have an effect on the grain segregation in polydispersed beds and bed stratification (Shiyuan *et al.*, 2010; Zhou *et al.*, 2011; Boer *et al.*, 2018; Cúñez and Franklin, 2019a). In particular, in fluidized beds used in wastwater treatment, biological films form around each particle, so that they tend to bound together in duos or trios. Therefore, the modeling of non-spherical particles started to draw a considerable amount of attention.

There are several ways of representing a non-spherical particle in DEM, but they can basically be divided in two main branches: the single-particle approach and the clustered-particle approach (Zhong *et al.*, 2016). In the first, the particle is one single solid described by a unique formulation, where the most common ones are the polyhedral (Hogue, 1998; Vollmari *et al.*, 2016), ellipsoidal (Zhou *et al.*, 2011) and the superquadric formulations (Hilton *et al.*, 2010; Podlozh-

nyuk *et al.*, 2017). Despite being relatively popular among non-spherical DEM simulations, these formulations demand expensive computational costs and complicated numerical algorithms to deal with the diverse contact scenarios. Besides, another great challenge in simulating non-spherical particles is to model correctly the drag force over the non-spherical body (Zastawny *et al.*, 2012; Ouchene *et al.*, 2015). One way to overcome these issues, is to use the clustered-particle approach, which is mainly restricted to multi-sphere models (Höhner *et al.*, 2011). In this method, complex shapes are represented by a combination of overlapping (Farivar *et al.*, 2020), simply connected (Chen *et al.*, 2015) or clumped spheres (Cho *et al.*, 2007). The latter takes into account the properties of the material that bond the spheres together and, therefore, is sometimes used to perform simulations of flexible fibers or to evaluate the mechanical properties of solid materials (Guo *et al.*, 2015; Quist and Evertsson, 2016). These models are easier to implement and uses a sphere-sphere contact algorithm, which is already validated for most of DEM softwares (Farivar *et al.*, 2020).

In this work, we investigate numerically the fluidization by water of non-spherical particles in narrow pipes, *i.e.* when the ratio between the pipe and the particle diameter is less than 50 (Cúñez and Franklin, 2019b). In such scenarios, the problem can become more complicated, because instabilities characterized by the formation of waves or plugs can occur (Anderson and Jackson, 1967; Cúñez and Franklin, 2019b). We present here the preliminary results considering each particle formed by three bonded spherical atoms in a triangle configuration. The main objectives are to understand the effect of non-sphericity on the physics of fluidized beds and develop a CFD-DEM methodology that can be further used to analyse analogous systems.

2. SIMULATION SETUP

The full three dimensional simulations are performed using the open source package CFDEM (Goniva *et al.*, 2012). It couples the well-known OpenFOAM CFD software, which is based on the finite volume method, with the LIGGGHTS code, employed for the DEM calculations. Both softwares are completely free and open source. The technical details of the simulations are presented in the next sections.

2.1 Mathematical formulation

There are two fundamentally possible formulations to couple the CFD and DEM models: namely the "Resolved" and the "Unresolved" approaches (Kloss *et al.*, 2012). Their choice depends mainly on how the scale of particles compares with the flow domain. If the particle diameter is small enough to fit in one computational cell, the unresolved formulation can be used. For fluidized bed simulations where narrow pipes are considered, the mesh size must be small enough to capture the main characteristics of the flow. In such cases, the particle diameter is usually larger than the cell size and, thus, the resolved formulation is more suitable. A resolved coupling demands a very refined mesh around the particles and, when a large number of particles is considered, it highly increases the computational cost of the simulation. One way to circumvent this problem is by using an unresolved approach referred to as "big particle model", where the region of influence of a particle is artificially increased and their volume increase is compensated by adding a fictitious porosity (Kloss *et al.*, 2012). In this formulation, the motion of the liquid is described by the incompressible volume-averaged Navier–Stokes equations (Kloss *et al.*, 2012):

$$\frac{\partial \alpha_f}{\partial t} + \nabla \cdot (\alpha_f \mathbf{u}_f) = 0 \tag{1}$$

$$\frac{\partial (\alpha_f \vec{u}_f)}{\partial t} + \nabla \cdot (\alpha_f \vec{u}_f \vec{u}_f) = -\alpha_f \nabla \frac{p}{\rho_f} - \vec{R}_{pf} + \frac{1}{\rho_f} \nabla \cdot \left(\alpha_f \vec{\bar{\tau}}_f \right) \tag{2}$$

where α_f is the volume fraction, $\vec{u}_f$ is the mean velocity, p is the pressure, ρ_f is the fluid density, $\vec{\bar{\tau}}_f$ is the stress tensor and $\vec{R}_{pf}$ is the particle-fluid momentum exchange due to drag force, given by (Mondal *et al.*, 2016):

$$\vec{R}_{pf} = \frac{\vec{K}_{pf}}{\rho_f} \left(\vec{u}_f - \langle \vec{u}_p \rangle \right) \tag{3}$$

where $\langle \vec{u}_p \rangle$ is the averaged particle velocity and $\vec{K}_{pf}$ is the implicit momentum exchange term between the solid and liquid phases:

$$\vec{K}_{pf} = \frac{\left| \sum_i \vec{F}_d \right|}{V_{cell} \left| \vec{u}_f - \langle \vec{u}_p \rangle \right|} \tag{4}$$

To calculate $\vec{K}_{pf}$, $\vec{F}_d$ was described by the Gidaspow drag correlation (Gidaspow *et al.*, 1991). This relation is given as a combination of the Wen and Yu model (Wen, 1966), when $\alpha_f > 0.8$, and the Ergun equation, (Ergun, 1952) when

$\alpha_f \leq 0.8$. For details see (Kloss *et al.*, 2012). The motion of solid particles is dictated by Newton's second law, using the linear and angular momentum equations, given by Eqs. 5 and 6, respectively (Cúñez and Franklin, 2019b):

$$m_p \frac{d\vec{u}_p}{dt} = \vec{F}_{pressure} - \vec{F}_d + \vec{F}_{vm} + \vec{F}_{\vec{g}} + \sum_{i \neq j}^{N_c} \left(\vec{F}_{c,ij}\right) + \sum_{i}^{N_w} \left(\vec{F}_{c,iw}\right) \tag{5}$$

$$I_p \frac{d\vec{\omega}_p}{dt} = \sum_{i \neq j}^{N_c} \left(\vec{T}_{p,ij}\right) + \sum_{i}^{N_w} \left(\vec{T}_{p,iw}\right) \tag{6}$$

where m_p is the mass of the particle, I_p is the moment of inertia, $\vec{\omega}_p$ is the angular velocity, $\vec{T}_p$ is the torque and $\vec{F}_{pressure}$, $\vec{F}_d$, $\vec{F}_{vm}$ and $\vec{F}_{\vec{g}}$ are the forces generated by the fluid pressure gradients, fluid drag, virtual mass, and gravity, respectively. The two last terms in the right-hand side of Eq. (5) are the particle-particle and the particle-wall contact forces, respectively.

The contact forces can be divided into two components, a normal $\vec{F}_{cn}$, given by Eq. 7, and a tangential $\vec{F}_{ct}$ one, Eq. 8. A spring-dashpot model based on a stiffness k, damping η, and friction $\mu_{fr,i}$ coefficients, is used to describe the contact forces (Cundall and Strack, 1979).

$$\vec{F}_{cn,ij} = \left(-k_n \delta_{nij}^{3/2} - \eta_n \vec{u}_{ij} \cdot \vec{n}_{ij}\right) \vec{n}_{ij} \tag{7}$$

$$\vec{F}_{ct,ij} = \left(-k_t \delta_{tij} - \eta_t \vec{u}_{sij} \cdot \vec{t}_{ij}\right) \vec{t}_{ij} \tag{8}$$

In the above equation the subscripts n and t represent the normal and tangential components, respectively. $\vec{n}_{ij}$ is the unit vector that connects the center of the particles, $\vec{u}_{ij}$ is the relative velocity between particles i and j, $\vec{u}_{sij}$ is the slip velocity at the contact point and $\vec{t}_{ij} = \vec{u}_{sij} / |\vec{u}_{sij}|$. Finally, the tangential overlap (sliding) of the particles at contact must satisfy a local frictional yield criterion, $\left|\vec{F}_{ct,ij}\right| > \mu_{fr} \left|\vec{F}_{cn,ij}\right|$ and $\vec{F}_{ct,ij} = -\mu_{fr} \left|\vec{F}_{cn,ij}\right| \vec{t}_{ij}$. The same equations presented in Eqs. 7 and 8 are applied to the particle-wall contact. Details regarding each force model can be found in (Cúñez and Franklin, 2019b,a).

The deformation of the bonds can also be described by its specific contact model (Guo *et al.*, 2013). Usually, the bond Young's modulus is considered to be lower than the one used for the particle to account for the elastic properties of the bond material (Shen *et al.*, 2016). However, in this work, for the sake of simplicity, the bond material is considered to be the same as the particle one, *i.e.*, a rigid material. Therefore, effects such as deformation or the breakup of bonds will not occur during the flow.

2.2 Problem description

We consider a water fluidized bed system consisting of 300 spherical atoms combined in a triangle formation. Figure 1 shows a sketch of the bonded particle used to perform the numerical simulations. The particles considered here are built from three identical spherical atoms, each with a diameter of d_p. The surface of each adjacent sphere is in contact and the spheres do not overlap. The bonds have a diameter of half of the diameter of the atoms and are considered to be solid, *i.e.* completely fill the internal space.

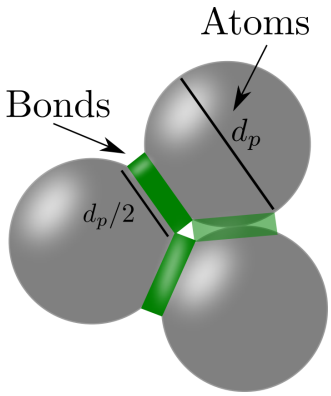

Figure 1. Sketch of the bonded particle used in the simulations

The spherical atoms are considered to be formed of aluminum and their properties are summarized in Tab. 1 (Cúñez and Franklin, 2019a). The different friction coefficients applied for the particle-particle contact $\mu_{fr,p}$ and the particle-wall contact $\mu_{fr,w}$ were used to account for the differences between the materials.

Table 1. Spherical atom and fluid physical properties

Atom diameter d_p (mm)	4.8
Atom density (kg/m^3)	2760
Young's modulus E (GPa)	71
Poisson ratio σ	0.34
Restitution coefficient e	0.5
Particle-particle friction coefficient $\mu_{fr,p}$	0.5
Particle-wall friction coefficient $\mu_{fr,w}$	0.9
Liquid density ρ_f (kg/m^3)	1000
Liquid viscosity μ_f $(Pa.s)$	0.001

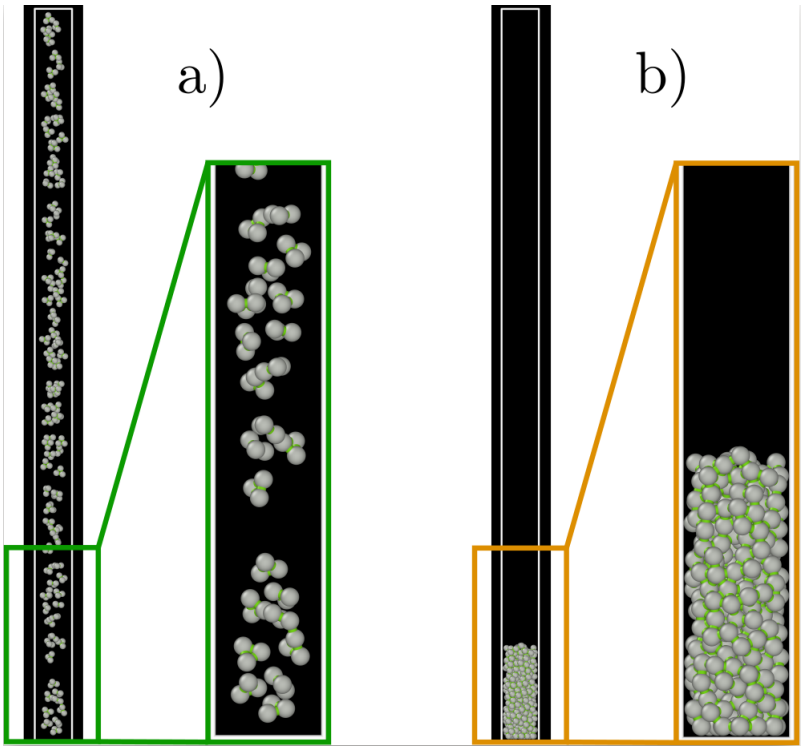

Figure 2. a) Initial random distribution of the bonded particles. b) Packed bed. Initial condition for the fluidization process.

The problem is initialized with a random distribution and orientation of the particles throughout a 25.4 mm diameter pipe of 0.55 m in length. At first, the particles are allowed to fall freely under water until a steady state is reached. Then, the ascendant flow rate slightly increases until it reaches a maximum value after 1 s. Here, we present the results for only one flow condition, which is given by a water flow mean velocity of $\bar{U} = 0.137m/s$, approximately $Q \approx 250L/h$. The initial particle distribution as well as the steady state packed bed are presented in Fig. 2

It is important to notice that the implementation of the bond formulation in LIGGGHTS has already been tested and validated against numerical and experimental results (Schramm *et al.*, 2019), and thus it is not discussed in this work.

2.3 Numerical setup

The problem is considered to be fully three-dimensional. For the walls on the side, a no-slip boundary condition for the fluid was imposed. At the inlet, the bottom boundary, we applied a zero gradient condition for the pressure. At the top, a zero gradient boundary condition was set for the velocity and a fixed value condition for the pressure. These conditions assume that a developed flow arrives at the exit of the pipe and generates a pressure gradient throughout the domain. The initial velocity is interpolated from zero to 0.137 m/s on the inlet over the first second of the simulation. This condition is more realistic and allows the bed to detach smoothly from the bottom boundary as the flow rate increases.

For the calculations, a computational mesh was built using the *blockMesh* utility of OpenFOAM. The mesh consisted of a total of 36,250 hexaedral cells, with a maximum cell volume of $\approx 1.15 \times 10^{-08} m^3$.

The equations are solved using a PISO (Pressure-Implicit with Splitting of Operators) pressure velocity coupling loop with two main pressure corrections and one non-orthogonal flux correction to account for the slightly non-orthogonal

cells generated by the cylindrical geometry. The DEM time-step was set to $1 \times 10^{-6} s$, which satisfies a 10% Rayleigh- and Hertz time scales. Usually, the DEM time steps are one order of magnitude smaller than that of CFD because of the dynamics of particle collision (Kloss *et al.*, 2012). For unresolved calculations, it is good practice to keep the coupling between the CFD-DEM time-steps around 50-100 DEM time-steps (Mondal *et al.*, 2016). So, to perform more accurate CFD simulations, the CFD time-step was set to $5 \times 10^{-5} s$, corresponding to 50 DEM time-steps.

3. PRELIMINARY RESULTS

Figure 3 shows snapshots of the bonded particles positions through time. In a first glance, it is possible to observe the formation of solid structures that collapse and regroup as they move upward in the pipe. Those compact regions are also known as plugs, and there have been few studies that tried to understand their dynamics, specially in confined systems (Cúñez and Franklin, 2019b). Besides the plug formation, some of the structures observed in the simulation of Fig. 3 sometimes get jammed while ascending. Cúñez and Franklin (2019b) showed how the contact forces propagate within the plugs and attain the tube wall and, thus, have a great influence on the plug formation. The same analysis can be employed here. However, in this case, the particles have a larger size combined with a non-spherical shape, which can induce other patterns than plugs, such as jams or even the pipe obstructions.

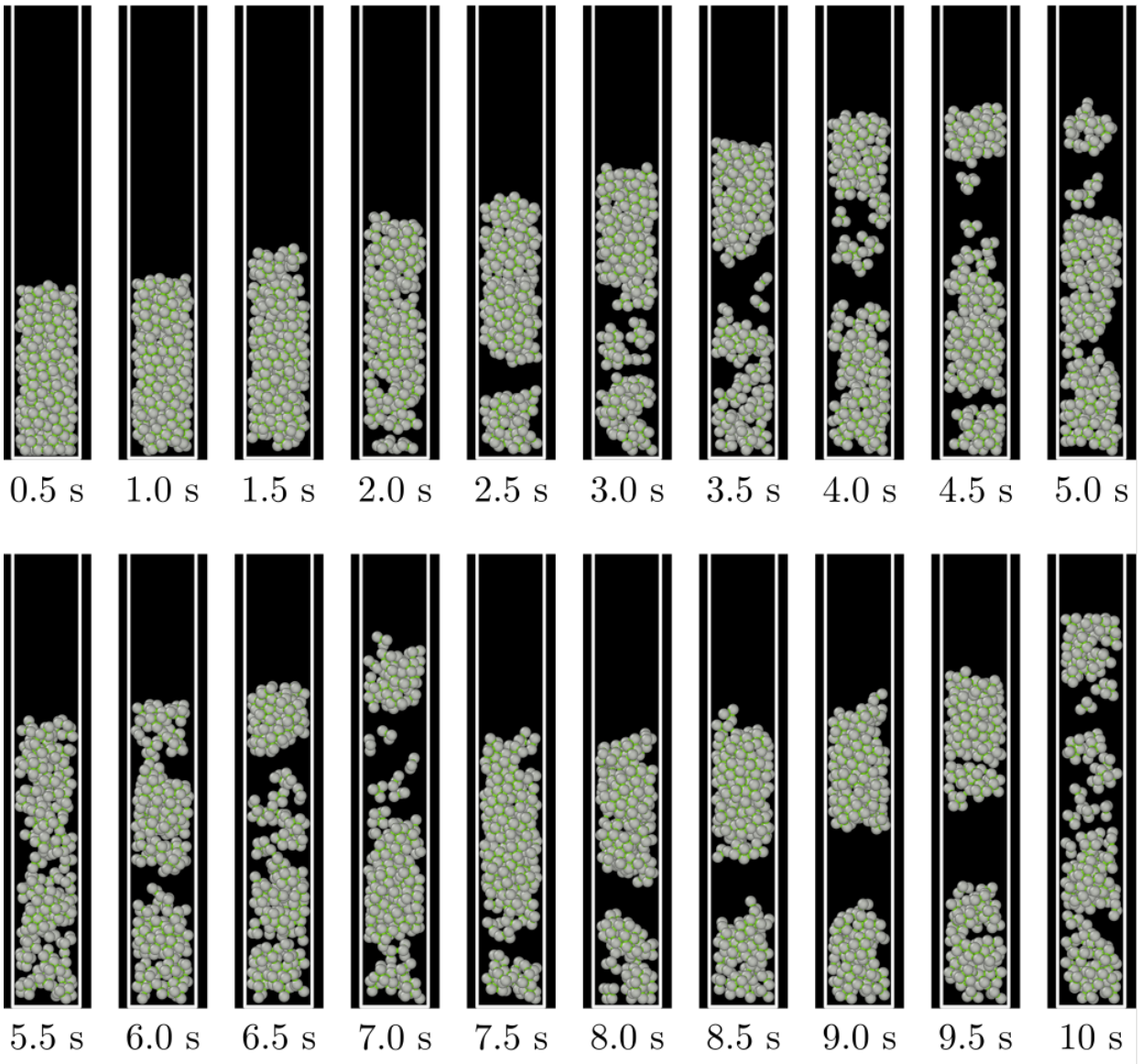

Figure 3. Evolution of the bed fluidization through time.

The particle's motion and structures from Fig. 3 were analysed by tracking each particle individually, and by checking the volume fraction distribution in different sections of the pipe. All the data was processed by means of numerical scripts (Cúñez and Franklin, 2019a) and specific plots were made to evaluate the average bed height, plug lengths and its upward

and downward velocities (bed celerities).

Figure 4 shows the plug evolution as a function of time, and the statistical distribution of the plug lengths. We can observe that, as the bed rises up, the plug slowly loses particles, decreasing in length (given by the difference between the blue and black symbols in Fig. 4a). Thereafter, the top of the bed drops quickly hitting a new ascending plug. The bed height varied from 0.08 m to 0.15, with an average value of 0.1164 m, and the plug length distribution shows an average of plugs around 0.039 m. Table 2 summarizes the results obtained by this numerical simulation and compare them with ongoing experiments. As we can see, the average parameters of the simulation present a maximum error compared to the experiments lower than 5% for all values except for the average plug length. Perhaps if we analyse a larger number of plugs, this result can be improved, once the initial random distribution of the particles also affects the results at the beginning of the fluidization process. Nevertheless, the preliminary results from the simulations are encouraging.

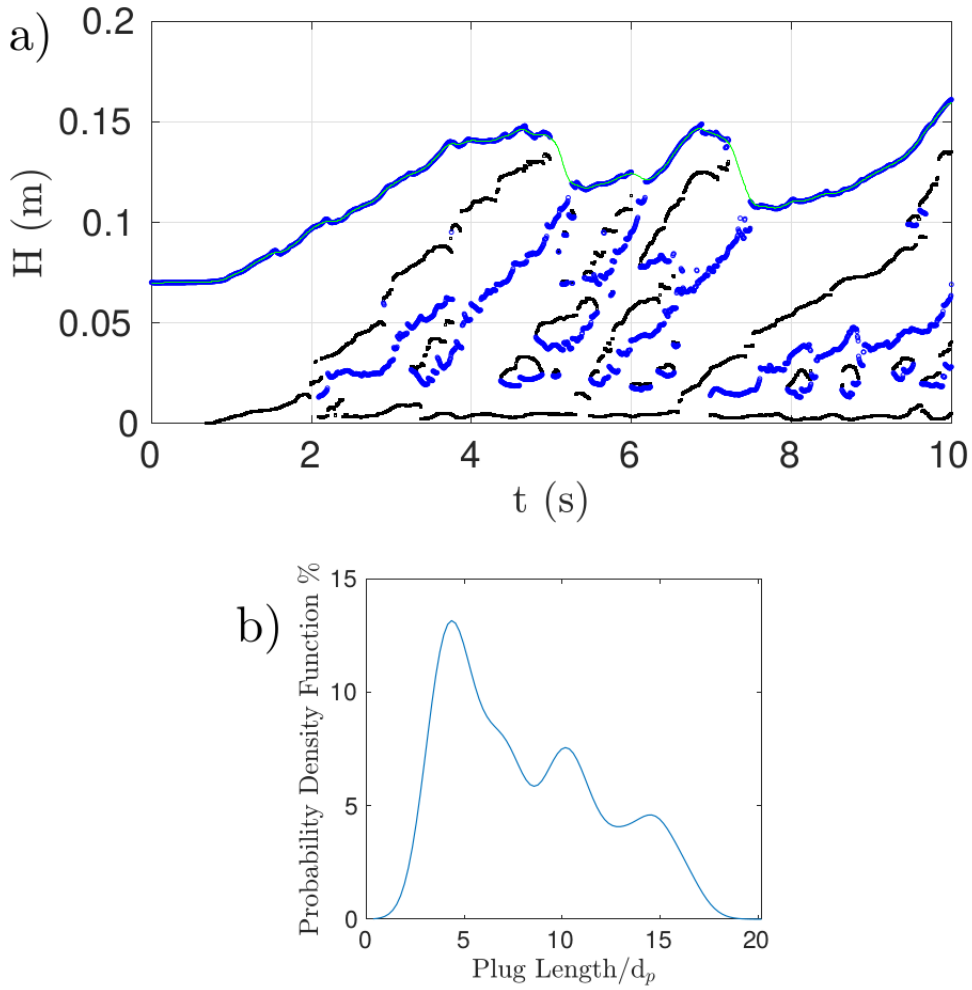

Figure 4. a) Plug evolution through time. Black symbols represent the start of the plug; blue symbols represent the end of the plug; green line is the averaged bed high. b) Probability density function of the plug lengths.

Table 2. Comparison between numerical simulation and experimental results.

Values	**Experiment**	**Numerical Simulations**	**Error %**
Average height of the fluidized bed (m)	0.1112	0.1164	4.68
Bed upward celerity (m/s)	0.0211	0.0207	1.90
Standard deviation of upward celerities (m/s)	0.0119	0.0146	22.69
Bed downward celerity (m/s)	-0.0325	-0.0331	1.85
Standard deviation of downward celerities (m/s)	0.0334	0.039	16.77
Length scale of plugs (m)	0.0338	0.0389	15.09
Standard deviation of length scale (m)	0.0197	0.0185	6.09

4. ACKNOWLEDGEMENT

The authors are grateful to the São Paulo Research Foundation - FAPESP (Grant Nos. 2019/20888-2, 2016/18189-0 and 2018/14981-7) for the financial support provided.

5. REFERENCES

Anderson, T.B. and Jackson, R., 1967. "Fluid mechanical description of fluidized beds. equations of motion". *Industrial & Engineering Chemistry Fundamentals*, Vol. 6, No. 4, pp. 527–539.

Boer, L., Buist, K., Deen, N., Padding, J.T. and Kuipers, J., 2018. "Experimental study on orientation and de-mixing phenomena of elongated particles in gas-fluidized beds". *Powder Technology*, Vol. 329, pp. 332–344.

Chen, Y., Third, J. and Müller, C., 2015. "A drag force correlation for approximately cubic particles constructed from identical spheres". *Chemical Engineering Science*, Vol. 123, pp. 146–154.

Cho, N.a., Martin, C. and Sego, D., 2007. "A clumped particle model for rock". *International journal of rock mechanics and mining sciences*, Vol. 44, No. 7, pp. 997–1010.

Cundall, P.A. and Strack, O.D., 1979. "A discrete numerical model for granular assemblies". *geotechnique*, Vol. 29, No. 1, pp. 47–65.

Cúñez, F.D.B. and Franklin, E.d.M., 2019a. "Mimicking layer inversion in solid-liquid fluidized beds in narrow tubes". *arXiv*, pp. arXiv–1912.

Cúñez, F.D.B. and Franklin, E.d.M., 2019b. "Plug regime in water fluidized beds in very narrow tubes". *Powder technology*, Vol. 345, pp. 234–246.

Deen, N., Annaland, M.V.S., Van der Hoef, M.A. and Kuipers, J., 2007. "Review of discrete particle modeling of fluidized beds". *Chemical engineering science*, Vol. 62, No. 1-2, pp. 28–44.

Didwania, A.K. and Homsy, G.M., 1981. "Flow regimes and flow transitions in liquid fluidized beds". *International Journal of Multiphase Flow*, Vol. 7, No. 6, pp. 563–580.

Ergun, S., 1952. "Fluid flow through packed columns". *Chem. Eng. Prog.*, Vol. 48, pp. 89–94.

Esteghamatian, A., Hammouti, A., Lance, M. and Wachs, A., 2017. "Particle resolved simulations of liquid/solid and gas/solid fluidized beds". *Physics of Fluids*, Vol. 29, No. 3, p. 033302.

Farivar, F., Zhang, H., Tian, Z.F. and Gupte, A., 2020. "Cfd-dem simulation of fluidization of multisphere-modelled cylindrical particles". *Powder Technology*, Vol. 360, pp. 1017–1027.

Gidaspow, D., Bezburuah, R. and Ding, J., 1991. "Hydrodynamics of circulating fluidized beds: kinetic theory approach". Technical report, Illinois Inst. of Tech., Chicago, IL (United States). Dept. of Chemical ....

Goniva, C., Kloss, C., Deen, N.G., Kuipers, J.A. and Pirker, S., 2012. "Influence of rolling friction on single spout fluidized bed simulation". *Particuology*, Vol. 10, No. 5, pp. 582–591.

Guazzelli, É., 2004. "Fluidized beds: from waves to bubbles". *The Physics of Granular Media*, pp. 211–232.

Guo, Y., Wassgren, C., Hancock, B., Ketterhagen, W. and Curtis, J., 2013. "Validation and time step determination of discrete element modeling of flexible fibers". *Powder technology*, Vol. 249, pp. 386–395.

Guo, Y., Wassgren, C., Hancock, B., Ketterhagen, W. and Curtis, J., 2015. "Computational study of granular shear flows of dry flexible fibres using the discrete element method". *Journal of Fluid Mechanics*, Vol. 775, pp. 24–52.

Hilton, J., Mason, L. and Cleary, P., 2010. "Dynamics of gas–solid fluidised beds with non-spherical particle geometry". *Chemical Engineering Science*, Vol. 65, No. 5, pp. 1584–1596.

Hogue, C., 1998. "Shape representation and contact detection for discrete element simulations of arbitrary geometries". *Engineering Computations*.

Höhner, D., Wirtz, S., Kruggel-Emden, H. and Scherer, V., 2011. "Comparison of the multi-sphere and polyhedral approach to simulate non-spherical particles within the discrete element method: Influence on temporal force evolution for multiple contacts". *Powder Technology*, Vol. 208, No. 3, pp. 643–656.

Kloss, C., Goniva, C., Hager, A., Amberger, S. and Pirker, S., 2012. "Models, algorithms and validation for opensource dem and cfd–dem". *Progress in Computational Fluid Dynamics, an International Journal*, Vol. 12, No. 2-3, pp. 140–152.

Mondal, S., Wu, C.H. and Sharma, M.M., 2016. "Coupled cfd-dem simulation of hydrodynamic bridging at constrictions". *International Journal of Multiphase Flow*, Vol. 84, pp. 245–263.

Nicolas, M., Chomaz, J.M., Vallet, D. and Guazzelli, E., 1996. "Experimental investigations on the nature of the first wavy instability in liquid-fluidized beds". *Physics of Fluids*, Vol. 8, No. 8, pp. 1987–1989.

Ouchene, R., Khalij, M., Tanière, A. and Arcen, B., 2015. "Drag, lift and torque coefficients for ellipsoidal particles: From low to moderate particle reynolds numbers". *Computers & fluids*, Vol. 113, pp. 53–64.

Podlozhnyuk, A., Pirker, S. and Kloss, C., 2017. "Efficient implementation of superquadric particles in discrete element method within an open-source framework". *Computational Particle Mechanics*, Vol. 4, No. 1, pp. 101–118.

Quist, J. and Evertsson, C.M., 2016. "Cone crusher modelling and simulation using dem". *Minerals Engineering*, Vol. 85, pp. 92–105.

Schramm, M., Tekeste, M.Z., Plouffe, C. and Harby, D., 2019. "Estimating bond damping and bond young's modulus for a flexible wheat straw discrete element method model". *Biosystems Engineering*, Vol. 186, pp. 349–355.

Shen, Z., Jiang, M. and Thornton, C., 2016. "Dem simulation of bonded granular material. part i: contact model and application to cemented sand". *Computers and Geotechnics*, Vol. 75, pp. 192–209.

Shiyuan, L., Qinggang, L. and Haipeng, T., 2010. "Agglomeration during fluidized-bed combustion of biomass".

Vollmari, K., Jasevičius, R. and Kruggel-Emden, H., 2016. "Experimental and numerical study of fluidization and pressure drop of spherical and non-spherical particles in a model scale fluidized bed". *Powder Technology*, Vol. 291, pp. 506–521.

Wen, C.Y., 1966. "Mechanics of fluidization". In *Chem. Eng. Prog. Symp. Ser.* Vol. 62, pp. 100–111.

Zastawny, M., Mallouppas, G., Zhao, F. and Van Wachem, B., 2012. "Derivation of drag and lift force and torque coefficients for non-spherical particles in flows". *International Journal of Multiphase Flow*, Vol. 39, pp. 227–239.

Zhong, W., Yu, A., Liu, X., Tong, Z. and Zhang, H., 2016. "Dem/cfd-dem modelling of non-spherical particulate systems: theoretical developments and applications". *Powder Technology*, Vol. 302, pp. 108–152.

Zhou, Z., Pinson, D., Zou, R. and Yu, A., 2011. "Discrete particle simulation of gas fluidization of ellipsoidal particles". *Chemical Engineering Science*, Vol. 66, No. 23, pp. 6128–6145.

6. RESPONSIBILITY NOTICE

The authors are solely responsible for the printed material included in this paper.